Available online at www.sciencedirect.com

SciVerse ScienceDirect

Procedia Engineering 58 (2013) 167 – 176

Procedia Engineering

www.elsevier.com/locate/procedia

The 12th Hypervelocity Impact Symposium

Large-scale Molecular Simulations of Hypervelocity Impact of Materials

Andres Jaramillo-Botero*, Qi An, Patrick L. Theofanis, and William A. Goddard III

California Institute of Technology, Materials and Process Simulation Center, 1200 E California Blvd, Pasadena, CA 91125, United States

Abstract

We describe the application of the ReaxFF reactive force field with short-range distance-dependent exponential inner wall corrections and the non-adiabatic electron Force Field (eFF) for studying the hypervelocity impact (HVI) effects on material properties. In particular, to understanding nonequilibrium energy/mass transfer, high strain/heat rate material decomposition, defects formation, plastic flow, phase transitions, and electronic excitation effects that arise from HVI impact of soft and hard materials on different material surfaces. Novel results are presented on the single shock Hugoniot and shock chemistry of Nylon6-6, on the hypervelocity shock sensitivity of energetic materials with planar interfacial defects and on HVI chemistry of silicon carbide surfaces with diamondoid nanoparticles. Both methods provide a means to elucidate the chemical, atomic and molecular processes that occur within the bulk and at the surfaces of materials subjected to HVI conditions and constitute a critical tool to enabling technologies required for the next□generation of energy, spatial, transportation, medical, and military systems and devices, among many others. This has proven to be extremely challenging, if not impossible, for experimental observations, mainly because the material states that occur are hard to isolate and their time scales for changes are too rapid (<1 ps). First□principles quantum mechanics (QM) simulation methods have also been bounded by the prohibitive scaling cost of propagating the total Schrödinger equation for more than 100 atoms at finite temperatures and pressures.

Selection and peer-review under responsibility of the Hypervelocity Impact Society

Keywords: Hypervelocity impact; Reactive molecular dynamics; Non-adiabatic molecular dynamics; Electronically excited states dynamics

1. Introduction

The atomistic mechanisms of the fundamental chemistry and physics of materials undergoing hypervelocity impacts (HVI > 2.5km/s) are challenging to investigate and still not well understood. The study of material phenomena under HVI conditions is especially relevant for space exploration and military use of space, where spaceships or projectiles are exposed to particulate hypervelocity collisions during their flight through low or high density atmospheres, cosmic dust or debris, that may result in surface degradation, on-board instrumentation failures due to impact plasma fields, or complete structural destruction. Spaceships and projectiles will need improved mechanical and thermal shielding materials to overcome the convective and radiative gas-surface flow conditions during atmospheric re-entry or during hypervelocity flight. HVI collisions are studied today by examining naturally occurring phenomena (e.g. in space), or via physical (e.g. using light gas guns, magnetic or laser fields, or linear motors to accelerate projectiles), and computational experiments. Unfortunately, the resolution of experimental measurements is significantly limited by the extreme conditions of pressure (Mbar range and strain-rates up to 10^{11}/s) and temperature (>kilo Kelvins) during HVI events. This grants a unique opportunity for computer simulations, albeit immense challenges as well. Important challenges for modeling include: welding, melting and vaporization, dissociation (fracture and fragmentation), ionization, and plasma formation; luminescence and radiative transport; deformation instabilities such as shear banding; hydrodynamic instabilities, mixed-phase flows, and – depending

* Corresponding author. Tel.: +1-626-395-3591; fax: +1-626-585-0918.
E-mail address: ajaramil@caltech.edu

1877-7058 © 2013 The Authors. Published by Elsevier Ltd.
Selection and peer-review under responsibility of the Hypervelocity Impact Society
doi:10.1016/j.proeng.2013.05.020

on material choices – mixing; solid-solid phase transitions, high-strain-rate deformation and thermo-mechanical coupling; and fracture, fragmentation, spall and ejecta [1-8]. In addition, during the early stages of compression extremely high strain rates associated with shock passage result in dynamic regimes that are extremely challenging to model.

Standard quantum mechanics (QM) methods provide an accurate description of geometries and energetics of barriers and reaction pathways in the ground state, but they are impractical for systems that require spatiotemporal resolutions to capture coupled chemical and mechanical degrees of freedom at finite temperatures and pressures or for modeling the dynamics of systems with a large number of electronically excited states; both of which are critical HVI conditions. The expected high-energy conditions during HVI events also render conventional molecular dynamics techniques and higher level continuum approximations useless in capturing bond breaking and formation or the effects of fast electronic transitions on material states. Breakthrough methods are sorely needed to cover "computational no-man's land" that falls in the regime of dynamics of materials with thousands to billions of atoms exposed to high temperature (10^3-10^5K) and Mbar pressures.

We address these issues with the first-principles-based reactive molecular dynamics (RMD) ReaxFF method, originally introduced in [9] and with the electron force field method (eFF) [10, 11]. ReaxFF provides nearly the accuracy of ground state quantum mechanics (QM) for describing reactive processes at the expense of conventional force fields. It enables the simulation of reactivity, diffusion, material decohesion and fragmentation, and phase transitions, which are essential to capturing the gas/surface chemistry and transport of molecular species during HVI events across the INMS surfaces. eFF on the other hand, is a mixed quantum-classical non-adiabatic solution to the time-dependent Schrodinger equation that enables an accurate description of large-scale non-adiabatic electronic processes, such as those expected from ionizing and excited electrons at high energy.

This paper is organized to introduce the reader to the key capabilities of ReaxFF and eFF, and to demonstrate new application problems in the study HVI phenomena. Concretely, we present preliminary results on the single shock Hugoniot and shock chemistry of Nylon6,6 and on the hypervelocity shock sensitivity of energetic materials with defects (planar interfaces) using ReaxFF, and on HVI of silicon carbide surfaces with diamondoid nanoparticles using eFF.

2. Hypervelocity impact simulations using reactive molecular dynamics

2.1. With the ReaxFF reactive force field

A critical deficiency in standard force fields is that they do not describe reactions accurately. ReaxFF allows bond formation, bond breaking, polarization, and reactions. This is critical for describing large-scale highly compressed states, equilibrium states, and dissociative processes. ReaxFF partitions the total interactions energy into valence, van der Waals (vdW), and electrostatic terms, just as in ordinary force fields (refer to [12] for more details). Distinct properties of our ReaxFF method for HVI include: charges are allowed to change every time step as bonds are formed or broken and they operate between all atoms, not just nonbonded ones; vdW interactions are included between all atoms, not just non-bonded atoms, allowing valence bonding interactions to be monotonically attractive; there are no predefined reactions or reaction pathways and the potential functions are able to automatically handle coordination changes associated with reactions; supports extremely high pressures, as those expected under HVI conditions, via a short-range distance-dependent exponential inner wall energy correction of the form $E_{inner} = D\exp\left(\alpha\left[1 - r_{ij}/r_{inner}\right]\right)$ where D, α, and r_{inner} are parameters fitted to high-compression QM data; incorporates a low gradient 2-body term of the form $E_{\lg} = -\sum_{ij,i<j}^{N} C_{\lg,ij} \Big/ \left(r_{ij}^6 + dR_{eij}^6\right)$ in the energy expression to account for London dispersions [13], thereby accurately describe volumes and phase transitions in molecular crystals (r_{ij} is the distance between atom i and atom j, R_{eij} is the equilibrium vdW distance between atoms i and j, and $C_{lg,ij}$ is the dispersion energy correction parameter, d is a scaling factor, set to 1.0 in most cases); all valence interactions, including bonds, angles and torsions, depend on the bond order (BO) and go to zero as the bonds are broken, and bond energy versus BO are determined to fit the bond dissociation and reaction pathways for a huge number of reactions; employs a 7th order distance-dependent Taper polynomial correction starting at r=0 and vanishing past r=10-12 Angstroms to avoid energy discontinuities when charged species move in and out of the non-bonded cutoff radius [12]; and all ReaxFF parameters are determined from a diverse set of QM data on structures (cell stresses, atomic RMS forces), charges, and differential energetics (complex parameter sets are now prepared using a new parallel hybrid genetic algorithm and conjugate gradient based optimization scheme, named Garffield for Genetic Algorithm based ReaxFF Force Field optimizer [14]).

The functional forms of ReaxFF provide accurate descriptions of transition states for a variety of allowed and forbidden reactions on an enormous number of reactions/structures and materials compositions, including H-Li, B-Ca, Ti, V, Fe-Zn, As-Rb, Y, Zr, Mo, Ru, Pd, In, Te, Xe, Bar, Hf-W, Pt, Au, Bi. ReaxFF has been applied extensively to simulate reactive systems and chemical events under relatively low energy conditions (<20eV). Recently we have demonstrated its use to

study the dynamics for hot-spot initiation at nonuniform interfaces of highly shocked materials [15], to predict equations of state for energetic materials [13], to study the thermal decomposition of condensed-phase nitromethane [16], to understand the mechanism and kinetics for the initial steps of pyrolysis and combustion of 1,6-Dicyclopropane-2,4-hexyne [17], to understand the dynamics of hydrocarbon chemisorption and decomposition [18], to characterize the hydration kinetics and mechanical response under hydrostatic pressure of the ettringite mineral in cement mixtures[19], and to study the hypervelocity impact fragmentation pathways of various organic molecules and ice clusters in space [20, 21].

2.1.1. Shock sensitivity in energetic materials

The interaction of shock waves with interfaces plays an essential role in the interfacial instabilities in inertial confinement fusion (ICF), in shock-induced Richtmyer-Meshkov instabilities (RMIs), and in detonation in heterogeneous polymer-bonded explosives (PBXs). Energetic materials are essential for applications ranging from rocket engines, to building and dam construction, and to armaments. Controlling the sensitivity of these materials in order to regulate unintentional detonation remains a challenge. In [22, 23] we demonstrated that ReaxFF leads to an accurate description of the complex chemistry of Energetic materials under shock-loading conditions. Hotspots result from defects in energetic material, such as voids, dislocation pileup, and other interfacial imperfections provide the starting point for explaining the initiation of rapid chemical decompositions and detonation[24-27]. In [15] we demonstrated hot-spot initiation at nonuniform interfaces in shocked polymer-bonded explosives (cyclotrimethylene trinitramine, RDX and hydroxyl-terminated polybutadiene, HTPB, model with 3,695,375 atoms/cell), here we use it to study hypervelocity shock induced hotspot formation on Pentaerythritol tetranitrate (PETN) with stacking faults (SF) in the (100) plane. We observe that a hot spot develops at the planar defect when the shock wave passes through. The hot spot is formed due to the coupling of shear flow and chemical reactions at the defects regions. This is the universal mechanism of hotspot formation in energetic materials with planar defects which is tested by examining the shock response for (100)/(110) interfaces of PETN.

We use gamma surfaces as a tool to extract the stacking faults and stacking faults energy (SFE) from our simulations. A gamma surface is the disregistry energy as a function of rigid shift of one half of the sample with respect to the other within the glide plane. We apply this concept on molecular crystal PETN by constructing a 6x3x3 supercell of perfect PETN crystal, then fixing one half and shifting (20 times) the other along the (010) and (001) directions in (100) surface. We then perform single point energy calculations on each shift of the half crystal to obtain a two dimensional gamma surface energy for the (100) plane. The results are shown in Fig. 1(A). These show a local minimum at dy = 5.16 Å and dz = 3 Å which corresponds to the possible stacking faults of the (100) plane with a stacking fault energy of 11.5 J/m2. To confirm this is a stable stacking fault structure, we minimized the energy of the structure and performed 12ps of constant pressure and temperature NPT-MD at T = 10 K and P = 1 atm. We then made a supercell of 24x12x12 with 200,448 atoms and size of 22.53x11.26x8.05 nm3 to study the dynamics of shock. We make the stacking fault on this supercell using the same method described above. The molecular arrangement after minimization and NPT-MD simulation of the shocked model is depicted in Fig. 1(B) and Fig. 1(C) (only C atoms are shown). We use the validated ReaxFF[15] and LAMMPS software[28, 29] to perform the shock simulations.

To simulate the propagation of shock waves in the PETN, we impacted the two-dimensionally PETN slab with stacking fault onto a reflective wall. The shock direction (x) was set to be finite. The slab was propelled at the desired impact velocity by adding a corresponding translational velocity on top of the thermal component. This procedure produces a shock wave with average particle velocity (U_p) equal to the impact velocity, propagating into the slab. A snapshot of the shock simulation is shown on Fig. 1(D) with atoms color-coded by maximum relative displacement (MRD).

From this setup, we explored the dynamic shock response of the mismatched interface in the PETN at U_p = 2.5 and 3.5 km/s via 5ps of adiabatic MD, at a time step of 0.1 femtoseconds. From the trajectories obtained during the RMD simulation we carried out a one-dimensional binning along the shock direction, at a bin resolution of 1 nm by 1 nm, to calculate the average temperature, normal stress and von-mises shear stress ($2\tau = \sigma_{xx}-(\sigma_{yy}+\sigma_{zz})/2$) in each bin. To track the chemical processes as the shock wave propagates through the PETN, we analyzed the fragments resulting from the corresponding trajectories based on a time-windowed (1 ps window size) average of bond orders. We then combined the fragment analysis results and the one-dimensional binning results, to examine the NO_2 dissociation in each bin at different stages of shock loading. To characterize the lattice deformation under shock loading conditions, we used the MRD slip vector, which has been shown to work for molecular crystal and polymers system[15, 30]. Next, we performed shock simulation on the PETN with stacking fault along the <100> direction to determine the temperature, stress, slip and chemistry profiles. Fig. 2 shows the time evolution of temperature T, normal stress σ_{xx}, shear stress τ and chemistry at arious stages of compression for U_p = 3.5 km/s. The temperature at the stacking fault region increases by ~300 K (21.4%) after the shock wave passes through compared to other shocked regions, leading to the formation of a hot spot (Fig. 2(A)). From the normal stress diagram (Fig. 2(B)) we find that a reflective wave forms when shock waves pass through the dislocations, due to the lattice mismatch. The normal stress at the hotspot regions is similar to other shocked regions even though the

reflective wave forms. The shear stress diagram also shows the same character of the reflected wave, which is similar to normal stress. The shear stress in the hotspot region decreases after the temperature increase and after most of the chemistry has taken place in the hotspot regions. The shear stress relaxation indicates a localized shear deformation in hotspot regions. Since NO_2 is the main product of HONO reactions in PETN decomposition, we examined the change in number of NO_2 species at the shocked region. The number of NO_2 in the hotspot regions increases dramatically after the hotspot forms. It is interesting to notice that NO_2 dissociation happened ~0.3 ps after the temperature increased, which indicates that the shear at the interface region caused the initial temperature rise which then leads to NO_2 bond breaking. The chemistry that happened in the hotspot regions led to an additional shear relaxation and a dramatic decrease of the shear stress.

Considering the high symmetry of PETN crystal, the center C atoms provide relevant information about packing under shock loading conditions. We use the MRD slip vector of center C atoms to characterize the shear deformation at the hotspot region. We examine the low shock velocity case at U_p = 2.5 km/s since little chemistry takes places at this speed. The cutoff of MRD is 9 Å which includes the first and second nearest neighbor molecules in PETN. The results indicate that the molecule has shear deformation at the (100) plane stacking fault regions when the shock wave passes through the fault, leading to hotspot formation and subsequently to chemical reactions followed by shear stress relaxation. We also notice a slip system at the (100) planes approximately along the <110> directions. For the cases of compressed shock wave loading through grain boundaries, such as (110)/(100), we also observed hotspot formation and shear deformation.

Our results indicate that shear deformation is an important and universal mechanism of hot spot formation in energetic materials with planar defects.

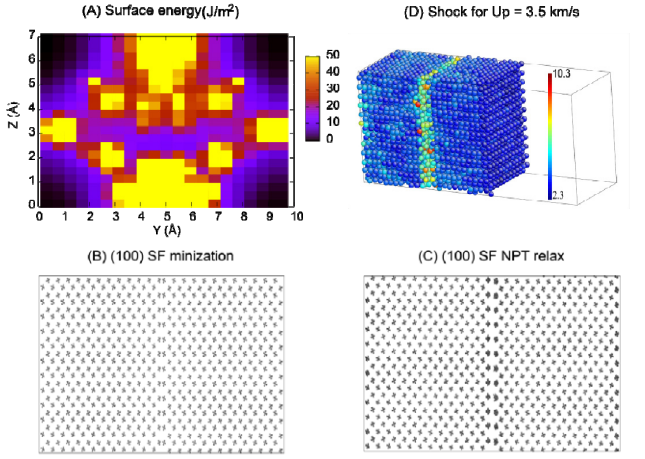

Fig. 2 Geometry of stacking faults and (100) surface energy in PETN model. (A) Stacking faults energy (SFE) of (100) plane; (B) Stacking faults structure after minimization; (C) Stacking fautls structure after NPT relaxation for 10ps; (D) shock response (color coded by MRD slip).

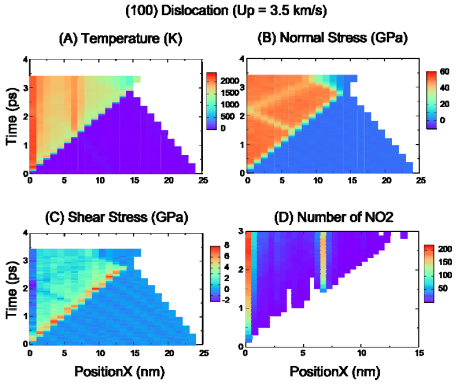

Fig. 1 X-time diagram of shocked (100) stacking faults in PETN. (A) Temperature: Hotspot forms as shock wave passes through the SF regions; (B) Normal stress: Reflective wave froms when shock wave reaches the SF region;(C) Shear stress: Shear stress decrease as hotspot forms and chemical reactions happened;(D) NO_2 distribution: Chemistry happened dramatically at Hotspot regions after temperature increases and shear deformation happened.

2.1.2. Shock in polymers (Nylon)

Polymers are used in inertial confinement fusion experiments, to contain fusion fuel (e.g. deuterium-tritium). By applying large amounts of energy, using lasers, onto a small spherical target fuel capsule it is imploded quickly to start fusion reactions. The capsule particles are contained from blowing apart by the inward inertia of the implosion, i.e. the implosion counteracts the explosion. But, as the fuel capsule compresses, the so-called Rayleigh-Taylor instabilities (RTI) cause small bumps or perturbations on the sphere or polymer-fuel interface of the capsule to grow, exponentially, in turn causing the spherical capsule geometry to become askew and the energy to be unevenly distributed. Sustaining fusion long enough is critical to yield as much power as was input during the implosion, hence understanding the polymer dynamics under high pressure is critical to control RTI in the design of efficient high-gain capsules for ICF.

We chose Nylon for our ReaxFF HVI models given its wide spread use in many other applications. Nylon-*m,n* has the general monomer structure –[-(NH-CO)-$(CH_2)_n$-2-(CO-NH)-$(CH_2)_m$-]-; we choose *m=6,n=6* for our model system. Current shock experiments on polyamide are up to pressures of 60 GPa, here we simulate the hypervelocity impact up to 10 km/s, which results in pressures ~200 GPa. Using the extended ReaxFF engine with inner wall and low gradient dispersion corrections, we ran NPT simulations on a triclinic 3x3x3 supercell model (with 4,104 atoms, similar to that reported in [31]) to confirm the crystal's lattice parameters (a=53.209,b=27.710,c=31.595,α=66.09, β=48,55, γ=82.24) and material density at room temperature of 1.29 g/cm^3 (experimental density is ~1.24 g/cm^3). Since the structure has an infinite chain along the *a* lattice direction, we rotated the crystal to align *a* with the *x* direction and the *a,b* plane with the *xy* plane, and made a 3x3x12 supercell with added vacuum padding (>20Angstroms) along the *z* direction; the chosen shock direction, perpendicular to the infinite chain direction. A reflective wall was introduced in the lowest *z* direction and a constant particle velocity was applied to the Nylon model in the direction of reflective wall. This procedure was repeated for a range of velocities between 1-10 km/s, and temperature, velocity and stress profiles were extracted from each run using a one-dimensional binning analysis in order to derive the shock wave velocity (U_s) profiles.

The resulting kinematics U_p-U_s relation and the corresponding Rankine-Hugoniot curves are shown in Fig. 3(A) and Fig. 3(B), respectively. Our ReaxFF calculated results are accurate within the existing experimental density and pressure ranges and predict a stiff increase in the Hugoniot pressures, as expected for this material. Fragment analysis of the shock trajectories reveal very limited chemical activity below 5km/s, which indicates chemical reactions are not significant within the region explored by published experiments (~60GPa). Reactions do become important when it exceeds this region and goes to higher pressure (Table 1).

As the velocities of impact increase to the point where electronic kinetic energy is commensurate with the potential energy interactions between electrons and nuclei (e.g. ionization) we have find that ReaxFF is no longer able to accurately capture the full chemistry and physics. Above this limit (~10-15km/s), we transition into the approach described next.

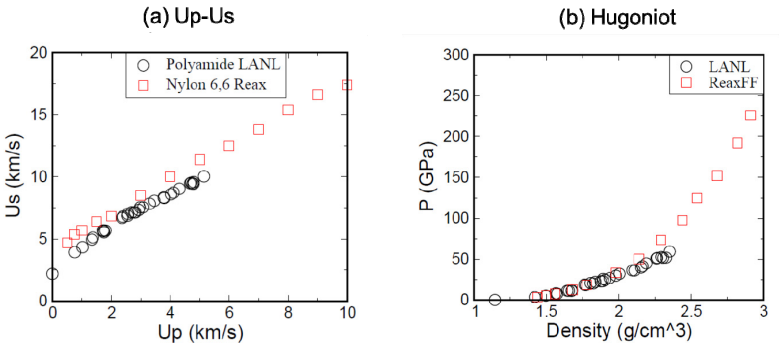

Fig. 3 Comparison of Up-Us relation and Hugoniot of nylon 6,6 crystal with experiment. The black circle results are from LANL experiment of polyamide. The red square results are from the ReaxFF hypervelocity impact simulations.

Table 1 Fragment analysis of hypervelocity impact of nylon 6,6 crystal. The initial crystal structure has 162 chains (C36H66N6O6)

V_{imp} (km/s)	H	H_2	C_2H_2O	OH	$C_{36}H_{66}N_6O_6$
5 (2ps)	4	1	0	1	142
7 (1ps)	10	49	20	36	20
10 (1ps)	398	1218	14	159	0

2.2. With the Electron Force Field (eFF)

The first-principles-based electron forcefield (eFF) is a mixed quantum-classical approach for studying nonadiabatic reactive dynamics based on floating spherical Gaussian wavepackets. eFF provides an approximate description of quantum dynamics by describing every electron as a floating spherical Gaussian orbital whose position and size varies dynamically while the nuclei are treated as classical point charge particles[32]. Here the total *N*-electron wavefunction is written as a Hartree product of one-electron orbitals (rather than as an explicitly antisymmetrized product). Orthogonality resulting from the Pauli Principle is enforced with a spin-dependent Pauli repulsion term in the systems Hamiltonian which is a function of the sizes and separations of these Gaussian orbitals. The Pauli potential accounts for the kinetic energy change due to orthogonalization, arising from the Pauli principle (antisymmetrization)[33]. An additional quantum-derived term in the eFF Hamiltonian is the kinetic energy for each orbital, which accounts for the Heisenberg principle. The full Hamiltonian in eFF also incorporates classical electrostatic terms between nuclei or electrons. For this study we used a parallel version of eFF, which is available in the official LAMMPS release as a user package[11, 28].

In the past, eFF was successfully applied to high-energy non-adiabatic processes such as Auger decay[34], H_2 in the warm dense matter regime[10], the hydrostatic[35] and dynamic[11] shock Hugoniot, exo-electron emission due to fracture in silicon[36], to study the dynamics of shocked amorphous and crystalline polyethylene[37], and to study the fragmentation pathways of organic molecules during HVI[21]. eFF is unique in that electronic and nuclear degrees of freedom evolve separately (i.e. non-adiabatic motion) and naturally while propagating the equations of motion orders of magnitude faster than with standard QM-MD methods, which allows us to perform millions of atoms scale and long-time-scale dynamics simulations[11].

2.2.1. Hypervelocity impact of diamondoid nanoparticles on SiC thin film surfaces

Here we describe the HVI impact of nanoparticles on silicon carbide (SiC). SiC is the only chemical compound of carbon and silicon. It has low density, high strength, low thermal expansion, high thermal conductivity, high hardness, high elastic modulus, and excellent thermal shock resistance with chemical inertness, so it is used today in numerous high-performance applications including abrasives, refractories, high quality technical grade ceramics, among others. It can also be made an electrical conductor and has applications in resistance heating and electronic components. Structural and wear applications are common in space re-entry vehicles because materials and systems must survive hypersonic conditions with exposure to intense radiation with highly reactive intermediates and ions. These conditions provide formidable challenges to all known materials and the experimental development of improved materials is hindered by the difficulty of land-based experiments that accurately reflect the conditions characteristic of a hypersonic re-entry vehicle in the upper atmosphere. One notable example was the conversion of the outer layers of the carbon fiber-reinforced carbon (RCC) material used in the nose cone and wing leading edges of the Space Shuttle orbiter into SiC to provide oxidation resistance for reuse capability. The next section presents preliminary investigations using eFF to explore the chemical, thermal and mechanical capabilities of SiC films to HVI.

For this study we prepared three simulation cells. In each cell, 3C-SiC is cleaved so that a rectangular slab with hydrogen-passivated (111) surfaces is produced. The cell is periodic in the *y* and *z* dimensions and finite in the *x* direction (which is parallel to [111]). The [111] direction contains 10 SiC bilayers, and the nominal proportions of the slab are 2.4 x 9.6 x 4.3 nm^3. In each cell the impactor is composed of a hydrogen-passivated carbon diamond sphere with a radius of 1.1 nm. Each impactor contains 84 carbon atoms, 88 hydrogen atoms, and 592 electrons. In total each simulation cell contains 5,040 silicon nuclei, 5,124 carbon nuclei, 1,096 hydrogen nuclei, and 52,000 electrons. This particular version of eFF uses an effective core potential for each silicon atom, so the number of electrons per silicon atom is limited to silicon's four valence electrons[36]. The three cells differ in the placement and ultimate direction of the impactor particle. We produced three impact angles: 0, 45, and 80 degrees off the surface normal vector with the impact site being set at the center of the slab. The impactor was initially placed laterally in the *y*-direction for the 45 and 80-degree impacts.

Electrons are placed around nuclei to mimic standard chemical bonding. Carbon 1s electrons are nuclei centered and they were given an initial radial value of 0.15 bohr. The core 1s, 2s, and 2p electrons of the silicon atoms are replaced by the effective core potential so they are omitted from the simulation. The valence electrons of each hydrogen, carbon, and silicon atom are "hybridized" into sp3 orbitals and they are arranged like σ-bonds directly between each bonded pair. C-H σ-bonds were initialized with a radius of 1.54 bohr and Si-H σ-bonds were given an initial radius of 1.81 Bohr. Si-Si and C-C σ-bonds were given initial radii of 1.92 and 1.28 Bohr, respectively.

Each cell was prepared by conjugate gradient energy minimization on the *x, y, z*, and radial degrees of freedom. The Nóse-Hoover thermostat and barostat was used to raise the temperature of each cell to 300 K and 1 atmosphere over the course of 2 picoseconds of NPT dynamics. After equilibration the impactor is given a total velocity of 10 or 20 km/s, and

constant volume and energy (NVE) dynamics are enforced so the system propagates as a microcanonical ensemble. Naturally the distribution of the *x*- and *y*-components of the velocity depend on the impact angle (see Fig. 4).

In the eFF method the electron mass is defined in three separate locations: 1) in the electronic kinetic energy, (i.e. wavefunction); 2) in the spin-dependent Pauli energy; and 3) in the equations of motion[11, 33]. The effect of modifying the electron mass in 1) and 2) affects the sizes of electrons in atoms and the lengths of bonds in molecules therefore we keep these fixed to avoid disrupting the chemistry of the system. In all potential energy terms the electron mass is set to the true electron mass (5.486×10^{-4} amu). The user may define a different dynamic electron mass to evolve the kinetic equations of motion[11, 33]. Changing the mass in the equations of motion varies the overall time scale of excited electron motions, with the time scale of excitation relaxations and energy transfer proportional to $m^{1/2}$. This is what we refer to as changing the dynamic masses. This does not affect the net partitioning of energy in the system nor the magnitude of the thermodynamic parameters we are interested in measuring. This does not alter the system's chemistry, just its evolution in time. An artificially heavy electron mass enables the use of longer integration time steps. For this study we set the dynamic electron mass to 1 amu. Because we used moderately heavy electrons we were able to use an integration timestep of 0.005 fs. The fast radial breathing modes of the carbon 1s electrons limits the integration timestep.

We examine the results of impacting a silicon carbide thin film with a harder, spherical diamond-like particle, at two velocities, 10 and 20 km/s, and three impact angles 0°, 45°, and 80°. eFF is unique among conventional force fields in that electrons are discrete particles, and this enables us to examine aspects of hypervelocity impact that other methods cannot. The eFF method allows us to measure damage on the atomistic scale, and we can obtain data regarding fragmentation, ionization, and heat diffusion. The range of impact velocities and angles we examined produced a variety of interesting results, some of which may be counterintuitive. As expected, the extent of the structural damage is directly proportional to the impact velocity and entry angle. 10 km/s orthogonal impacts produced partial melting at the interface of the diamondoid impactor particle and the silicon carbide surface. The impactor collided with the surface, reversed momentum, and became a hot amorphous semi-liquid. The impactor welded to the surface due to melting. Interestingly, the impactor assumed a droplet shape with necking near the surface due to the reversal of momentum after the collision (see Fig. 5, top left). The oblique impacts produced rebounding collisions. When the impactor strikes the silicon carbide surface at 10 km/s at an angle 45° off the surface normal it rebounds off the surface and lightly etches the surface. Silicon and carbon atoms from the first surface bilayer are ejected following the impactor. A 10 km/s impact with a very shallow impact angle of 80° caused the impactor to rebound and fragment off the surface. The only damage to the material is caused by the shock wave that follows the collision, and this damage is transient. The silicon carbide thin film reverts to its normal crystalline structure after the impact event. The impactor however fragments and ionized nuclei and electrons are ejected.

At 20 km/s the damage to the thin film is far more substantial. At an impact angle of 0°, the impactor easily penetrated the SiC thin film. The impactor produced a 17Å perforation, and it was able to penetrate 6 bilayers of the film. The 45° impact also caused penetration of the film. Because the impactor had substantial lateral momentum, it was able to drag atoms with it and this contributed to it producing a 20Å perforation. With an impact angle of 80°, the impactor did not penetrate the surface, but it caused significant etching. Atoms from the first 2 bilayers were removed from the surface. In all cases the impact caused a cascade of ionized particles to be ejected from the surface, and electrons within the bulk were also ionized.

Figure 5 shows the number of ionized particles in each cell at each point in the impact simulations. In Fig. 5(a) the results from collisions at 10 km/s are presented. The initial impact happens just before 200 fs, and the first wave of ionizations are mostly attributed to fragmentation of the impactor. Near 600 fs, ionization is attenuated, and another wave of ionization begins. The ionization wave between 600 and 1300 fs is due to the passage of shock waves in the SiC film. The first peak

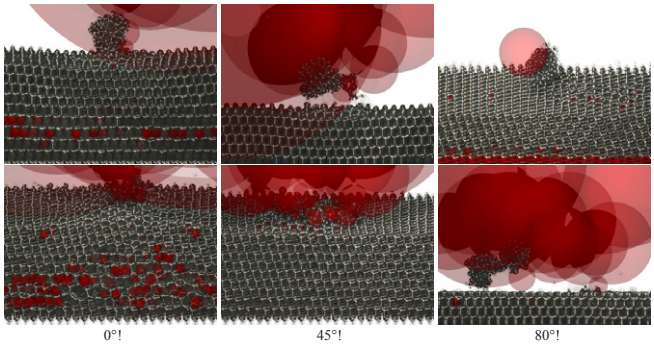

Fig. 4. Snapshots of the impact simulations. Top row: 10 km/s impacts. Bottom row: 20 km/s impacts. The transparent red spheres are ionized/diffuse electrons.

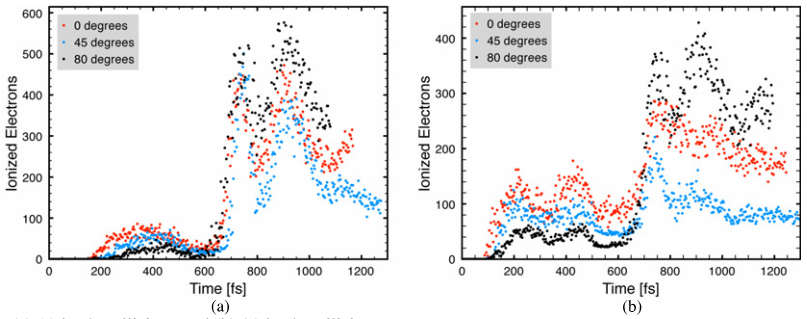

Fig. 5. Ionization yields for (a) 10 km/s collisions and (b) 20 km/s collisions.

near 750 fs corresponds to the collision shock wave compressing and heating the film. As the film relaxes, so do the electrons. However, a rarefaction wave emanates from the fixed bottom layer and initiates a second round of ionization that peaks near 900 fs. While this is an artifact of the fixed bottom layer, it is reasonable to expect a shock impedance mismatch between the SiC layer and whatever material is beneath it in real world applications. This mismatch would also cause a rarefaction wave. A similar trend is observed for the 20 km/s impacts in Fig. 5(b). Ionization begins near 100 fs since the impactor is traveling twice as fast. The ionization rate is higher because the impacts are more energetic. In this initial ionization event, a greater number of impactor electrons are lost in the void above the slab, and this is evident in the jet of ejecta. As the impactor is stopped near 500 fs, the ionization rate slows and some electrons relax and become bound again. Just like the 10 km/s collisions, ionization due to the passage of shock waves and rarefaction waves can be detected between 700 and 1200 fs. Interestingly, in this event, the total number of ionized particles is lower for the 20 km/s impacts than for the 10 km/s impacts. This is likely due to the fact that the impactor is able to more deeply penetrate the SiC film. Additionally, a greater number of electrons are ionized earlier in the simulations. Ionized electrons are effectively trapped and they can form bonds between the melted diamondoid slug and the damaged SiC film.

Figure 6 shows the heat dissipation during each impact simulation. The temperatures plotted are the average of the entire simulation cell including the translational impactor particle contributions. Two distinct domains characterize the heat dissipation behavior during the HVI: the stopping domain and the shock wave propagation domain. The stopping domain occurs between the moment of impact, ~200 fs for 10 km/s impacts (Fig. 6 left) and 100 fs for 20 km/s impacts (Fig. 6 right) and the moment the momentum of the impactor is either slowed or reversed. The shock wave propagation domain is the time in which the impact shock wave traverses the cell. Energy is dissipated throughout the cell by excitation of phonon modes that couple with the shock wave. In the 10 km/s regime the 0° and 45° impacts are able to dissipate heat at a rate of 27 K/fs in the stopping phase and then 0.75 K/fs in the shock phase. The 80° cell remains hot after impact because little energy is absorbed by the thin film during the oblique impact event. The impactor is hardly slowed, and this skews the average temperature of the cell upwards. The thin film is able to stop the impactor during 20 km/s, 0° and 45° impacts, though it dissipates heat energy at a rate of 90 K/fs in doing so. Interestingly, in the 20 km/s regime, 0° and 45° impacts quickly dissipate energy in the shock phase. After the impactor is arrested, only 500 fs elapse before the cell temperature equilibrates to a value of 550 K. This corresponds to a dissipation rate of 3 K/fs. This could be because a greater number of electrons are ionized in the stopping phase, and energy is dissipated more effectively by thermal excitation of electrons than by phonon excitation and scattering. We are currently performing simulations on much larger slabs with eFF, using different impactor compositions, to determine the chemical and mechanical imprint of SiC during HVI. This will be the subject of a different publication.

3. Concluding remarks

We know of no current alternate technologies to ReaxFF and eFF for accurately capturing the full range of phenomena that appear under the extreme conditions of hypervelocity impact. Standard QM is limited both by the length (a few hundred atoms) and time scales (<1ps for QM-MD) of simulation. Density functional theory (DFT), the primary QM workhorse is also an adiabatic method with very limited capabilities for handling a large number of electronic excitations at finite temperatures (i.e. using curve hoping techniques or time-dependent-DFT variants). At extreme high pressures Path Integral Monte Carlo schemes are capable of statistically sampling thermodynamic states but cannot describe critical dynamic phenomena during HVI. Conventional force fields on the other hand, can handle the length and time scales required in these simulations, but cannot handle reaction processes nor high-energy states of mater.

ReaxFF addresses the highly compressed and dissociative states that cannot be described with conventional force fields techniques from molecular dynamics under an adiabatic approximation (<20eV), and eFF the breakdown of the

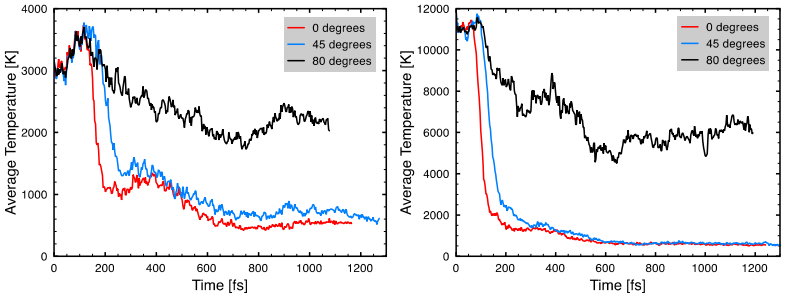

Fig. 6. Heat dissipation during the impact simulations. Left: 10 km/s impacts, and right: 20 km/s impacts.

Born□Oppenheimer approximation in the limit of a large number of electronic excitations (up to 100's of eV), where the electronic portion of the wavefunction contains contributions from many stationary states. The use of ReaxFF for HVI in the range of velocities that don't cause significant ionization enables calculations with nearly QM accuracy for large-scale molecular dynamics simulations of chemical reactions under extreme conditions of pressure and temperature, including nonequilibrium energy/mass transfer, decomposition under high strain/heat rates, defects formation, plastic flow, and phase transitions. The inner wall along with the low gradient dispersion corrections to ReaxFF, fitted to QM for highly compressed conditions, provide QM accuracy at the distances encountered during high-speed collisions. Here, we have shown its use to understand the effects of chemistry at high pressures and temperatures for two important applications.

In the upper limit of temperature and pressure for ReaxFF, eFF serves as a unique approach for computing the properties of materials in extreme conditions and tracing the system dynamics over multi-picosend timescales; this is particularly relevant where electron excitations can change significantly the nature of bonding in the system as expected during HVI. It can capture with surprising accuracy the behavior of such systems because it describes consistently and in an unbiased manner many different kinds of bonds, including covalent, ionic, multicenter, ionic, and plasma, and how they interconvert and/or change when they become excited. eFF effective core potentials (e.g. for Si) reduce the inaccuracies introduced from non-spherical high-energy electrons and reduce the overall computational cost of calculations. For systems at very high temperatures (hundreds of thousands of Kelvin) an ideal gas correction to recover the correct EOS is needed since the eFF wave packets will become very diffuse and no longer interact with the remainder of the system; hence all pressure contribution from the electrons is lost. The preliminary results reported here for Nylon and PETN are in close agreement with experimental data, while the SiC results remain exploratory considering the lack of experimental or QM evidence.

Acknowledgements

This work was performed at the Caltech with partial support from the Department of Energy National Nuclear Security Administration (NNSA) under award number DE-FC52-08NA28613, Army Research Office (ARO) under award number W911NF-05-1-0345 and W911NF-08-1-0124, and the Office of Naval Research (ONR) under award number N00014-09-1-0634. Computations were carried out on the Los Alamos (LANL), Army HPC systems and the soft matter simulation CPU/GPU cluster at Caltech (NSF award 1040558). We thank Dr. Sergey Zybin for his input in the PETN work and Dr. Betsy Rice and Larry Davis for their assistance.

References

1. Jean, B. and T.L. Rollins, *Radiation from Hypervelocity Impact Generated Plasma.* Aiaa Journal, 1970. **8**(10): p. 1742-&.
2. Eichhorn, G., *Measurements of Light Flash Produced by High-Velocity Particle Impact.* Planetary and Space Science, 1975. **23**(11): p. 1519-1525.
3. Eichhorn, G., *Analysis of Hypervelocity Impact Process from Impact Flash Measurements.* Planetary and Space Science, 1976. **24**(8): p. 771-&.
4. Eichhorn, G., *Heating and Vaporization during Hyper-Velocity Particle Impact.* Planetary and Space Science, 1978. **26**(5): p. 463-467.
5. Eichhorn, G., *Primary Velocity Dependence of Impact Ejecta Parameters.* Planetary and Space Science, 1978. **26**(5): p. 469-471.
6. Chhabildas, L.C., W.D. Reinhart, T.F. Thornhill, G.C. Bessette, W.V. Saul, R.J. Lawrence, and M.E. Kipp, *Debris generation and propagation phenomenology from hypervelocity impacts on aluminum from 6 to 11 km/s.* International Journal of Impact Engineering, 2003. **29**(1-10): p. 185-202.
7. Lawrence, R.J., W.A. Reinhart, L.C. Chhabildas, and T.F. Thornhill, *Hypervelocity impact flash at 6, 11, and 25 KM/S.* Shock Compression of Condensed Matter - 2005, Pts 1 and 2, 2006. **845**: p. 1349-1352.
8. Lawrence, R.J., W.D. Reinhart, L.C. Chhabildas, and T.F. Thornhill, *Spectral measurements of hypervelocity impact flash.*

International Journal of Impact Engineering, 2006. **33**(1-12): p. 353-363.
9. van Duin, A.C.T., S. Dasgupta, F. Lorant, and W.A. Goddard, *ReaxFF: A reactive force field for hydrocarbons.* Journal of Physical Chemistry A, 2001. **105**(41): p. 9396-9409.
10. Su, J.T. and W.A. Goddard, *Excited electron dynamics modeling of warm dense matter.* Physical Review Letters, 2007. **99**(18): p. 4.
11. Jaramillo-Botero, A., J. Su, A. Qi, and W.A. Goddard, *Large-Scale, Long-Term Nonadiabatic Electron Molecular Dynamics for Describing Material Properties and Phenomena in Extreme Environments.* Journal of Computational Chemistry, 2011. **32**(3): p. 497-512.
12. Chenoweth, K., A.C.T. van Duin, and W.A. Goddard, *ReaxFF reactive force field for molecular dynamics simulations of hydrocarbon oxidation.* Journal of Physical Chemistry A, 2008. **112**(5): p. 1040-1053.
13. Liu, L.C., Y. Liu, S.V. Zybin, H. Sun, and W.A. Goddard, *ReaxFF-/g: Correction of the ReaxFF Reactive Force Field for London Dispersion, with Applications to the Equations of State for Energetic Materials.* Journal of Physical Chemistry A, 2011. **115**(40): p. 11016-11022.
14. Jaramillo-Botero, A., *Garrfield: Genetic Algorithm based ReaxFF Force Field Optimizer*, 2012, California Institute of Technology: Pasadena.
15. An, Q., S.V. Zybin, W.A. Goddard, A. Jaramillo-Botero, M. Blanco, and S.N. Luo, *Elucidation of the dynamics for hot-spot initiation at nonuniform interfaces of highly shocked materials.* Physical Review B, 2011. **84**(22).
16. Han, S.P., A.C.T. van Duin, W.A. Goddard, and A. Strachan, *Thermal Decomposition of Condensed-Phase Nitromethane from Molecular Dynamics from ReaxFF Reactive Dynamics.* Journal of Physical Chemistry B, 2011. **115**(20): p. 6534-6540.
17. Liu, L.C., C. Bai, H. Sun, and W.A. Goddard, *Mechanism and Kinetics for the Initial Steps of Pyrolysis and Combustion of 1,6-Dicyclopropane-2,4-hexyne from ReaxFF Reactive Dynamics.* Journal of Physical Chemistry A, 2011. **115**(19): p. 4941-4950.
18. Mueller, J.E., A.C.T. van Duin, and W.A. Goddard, *Development and Validation of ReaxFF Reactive Force Field for Hydrocarbon Chemistry Catalyzed by Nickel.* Journal of Physical Chemistry C, 2010. **114**(11): p. 4939-4949.
19. Liu, L.C., A. Jaramillo-Botero, W.A. Goddard, and H. Sun, *Development of a ReaxFF Reactive Force Field for Ettringite and Study of its Mechanical Failure Modes from Reactive Dynamics Simulations.* Journal of Physical Chemistry A, 2012. **116**(15): p. 3918-3925.
20. Jaramillo-Botero, A. *Hypervelocity impact fragmentation of molecules*. in *MSC Annual Research Conference 2012*. 2012. Caltech.
21. Jaramillo-Botero, A., Q. An, M.J. Cheng, L.W. Beegle, R. Hodyss, and W.A. Goddard, *Hypervelocity Impact Effect of Molecules from Enceladus' Plume and Titan's Upper Atmosphere on NASA's Cassini Spectrometer from Reactive Dynamics Simulations.* Under review Phys. Rev. Letters, March 2012, 2012.
22. Nomura, K.I., R.K. Kalia, A. Nakano, P. Vashishta, A.C.T. van Duin, and W.A. Goddard, *Dynamic transition in the structure of an energetic crystal during chemical reactions at shock front prior to detonation.* Physical Review Letters, 2007. **99**(14).
23. Zybin, S.V., W.A. Goddard, P. Xu, A.C.T. van Duin, and A.P. Thompson, *Physical mechanism of anisotropic sensitivity in pentaerythritol tetranitrate from compressive-shear reaction dynamics simulations.* Applied Physics Letters, 2010. **96**(8).
24. Armstrong, R.W., *Dislocation Mechanics Aspects of Energetic Material Composites.* Reviews on Advanced Materials Science, 2009. **19**(1-2): p. 13-40.
25. Dear, J.P., J.E. Field, and A.J. Walton, *Gas-Compression and Jet Formation in Cavities Collapsed by a Shock-Wave.* Nature, 1988. **332**(6164): p. 505-508.
26. Field, J.E., *Hot-Spot Ignition Mechanisms for Explosives.* Accounts of Chemical Research, 1992. **25**(11): p. 489-496.
27. Holian, B.L., T.C. Germann, J.B. Maillet, and C.T. White, *Atomistic mechanism for hot spot initiation.* Physical Review Letters, 2002. **89**(28).
28. Plimpton, S., *Fast Parallel Algorithms for Short-Range Molecular-Dynamics.* Journal of Computational Physics, 1995. **117**(1): p. 1-19.
29. Aktulga, H.M., J.C. Fogarty, S.A. Pandit, and A.Y. Grama, *Parallel reactive molecular dynamics: Numerical methods and algorithmic techniques.* Parallel Computing, 2012. **38**(4-5): p. 245-259.
30. Zimmerman, J.A., C.L. Kelchner, P.A. Klein, J.C. Hamilton, and S.M. Foiles, *Surface step effects on nanoindentation.* Physical Review Letters, 2001. **87**(16): p. art. no.-165507.
31. Dasgupta, S., W.B. Hammond, and W.A. Goddard, *Crystal structures and properties of nylon polymers from theory.* Journal of the American Chemical Society, 1996. **118**(49): p. 12291-12301.
32. Frost, A.A., *Floating Spherical Gaussian Orbital Model of Molecular Structure .I. Computational Procedure . Lih as an Example.* Journal of Chemical Physics, 1967. **47**(10): p. 3707-&.
33. Su, J., *An electron force field for simulating large scale excited electron dynamics*, in *Chemistry and Chemical Engineering*2007, California Institute of Technology: Pasadena.
34. Su, J.T. and W.A. Goddard, *Mechanisms of Auger-induced chemistry derived from wave packet dynamics.* Proceedings of the National Academy of Sciences of the United States of America, 2009. **106**(4): p. 1001-1005.
35. Kim, H., J.T. Su, and W.A. Goddard, *High-temperature high-pressure phases of lithium from electron force field (eFF) quantum electron dynamics simulations.* Proceedings of the National Academy of Sciences of the United States of America, 2011. **108**(37): p. 15101-15105.
36. Theofanis, P.L., A. Jaramillo-Botero, W.A. Goddard, and H. Xiao, *Nonadiabatic Study of Dynamic Electronic Effects during Brittle Fracture of Silicon.* Physical Review Letters, 2012. **108**(4).
37. Theofanis, P.L., A. Jaramillo-Botero, W.A. Goddard, T.R. Mattsson, and A.P. Thompson, *Electron dynamics of shocked polyethylene crystal.* Physical Review B, 2012. **85**(9).